Fractional-Electron and Transition-Potential Methods for Core-to-Valence Excitation Energies Using Density Functional Theory

Subrata Jana and John M. Herbert*
Department of Chemistry and Biochemistry, The Ohio State University, Columbus, Ohio 43210 USA
(Dated: June 12, 2023)

Methods for computing x-ray absorption spectra based on a constrained core hole (possibly containing a fractional electron) are examined. These methods are based on Slater's transition concept and its generalizations, wherein core-to-valence excitation energies are determined using Kohn-Sham orbital energies. The transition-potential approximation avoids promoting electrons beyond the lowest unoccupied molecular orbital, facilitating robust convergence. Variants of these ideas are systematically tested, revealing a best-case accuracy of 0.3–0.4 eV (with respect to experiment) for K-edge transition energies. Absolute errors are much larger for higher-lying near-edge transitions but can be reduced below 1 eV by introducing an empirical shift based on a charge-neutral transition-potential method, in conjunction with functionals such as SCAN, SCAN0, or B3LYP. This procedure affords an entire excitation spectrum from a single fractional-electron calculation, at the cost of ground-state density functional theory and without the need for state-by-state calculations. This shifted transition-potential approach may be especially useful for simulating transient spectroscopies or in complex systems where excited-state Kohn-Sham calculations are challenging.

1 Introduction

X-ray absorption spectroscopy (XAS) is a powerful tool to elucidate structural and dynamical information for atoms, molecules, solids, and materials.[1–5] Due to the localized nature of core orbitals, XAS provides element-specific information while maintaining sensitivity to chemical environment.[4–12] Theoretical calculations of core-to-valence transition energies are invaluable for interpreting such spectra.[13–22] Available computational models include time-dependent density functional theory (TD-DFT),[19–24] orbital-optimized excited-state DFT,[18–21,25–28] correlated wave function models,[29–32] and the Bethe-Salpeter equation (BSE) approach.[33–37] Each of these methods is widely used and available in standard electronic structure codes, but there are limitations. Not least among these is cost, and only the DFT-based approaches are scalable to large systems such as proteins or liquid environments. Excited-state DFT methods, which are based on finding a non-*Aufbau* solution to the Kohn-Sham equations,[21] require tedious state-by-state calculations if an entire excitation spectrum is desired. In contrast, TD-DFT can furnish the entire core-level spectrum in a single shot (when used with frozen occupied orbitals for the valence electrons),[19–21] but absolute errors are often > 10 eV for light elements[38–41] and much larger for heavier ones.[42,43]

Building on previous work,[44] we seek simplified approaches based on Kohn-Sham eigenvalues only. These encode information regarding chemical shifts and may be useful in modeling emerging transient spectroscopies at x-ray and extreme ultraviolet wavelengths.[45–50] Thus, we investigate "core-hole constraining" methods for XAS that are based on time-independent (ground-state) DFT calculations. There are several variants,[18,51] as described in Section 2, and the unifying feature of these methods is that an electron or a fraction of an electron is removed from a core orbital, then orbital relaxation is incorporated by solving the Kohn-Sham equations in the presence of a (possibly fractional) core hole. Core-to-valence excitation energies

$$\omega_{v\to c} = \varepsilon_v - \varepsilon_c \tag{1}$$

are estimated as differences between final-state (virtual) energy levels ε_v and the initial-state (core) level, ε_c. In some cases, a fractional electron may be placed into the lowest unoccupied molecular orbital (LUMO), as described in Section 2, but not to higher-lying virtual MOs. Transition intensities are computed according to

$$I_{v\to c} = \frac{2m_e\omega_{v\to c}}{3e^2\hbar}\left\|\langle\psi_v|\hat{\boldsymbol{\mu}}|\psi_c\rangle\right\|^2 . \tag{2}$$

The signature of these approaches is that no proper excited-state calculation is performed. Instead, the requisite information for XAS is extracted from ground-state MOs and their energy levels.

The description above encompasses a variety of eigenvalue-based approaches that include Slater's transition method (STM)[52–56] and its generalizations.[44,51,57–60] Also considered is the transition potential method (TPM)[18,61–63] and generalizations thereof,[18,51,64] which are more convenient and robust as compared to Slater's original idea, along with the full core-hole method (FCHM).[18,65–67] Some of these methods are based on the use of fractional-electron self-consistent field (SCF) calculations.[18,51] They differ in whether the virtual orbitals are probed one by one, as in Slater's original conception, or whether the virtual orbital energy levels (ε_v) are obtained from a single calculation. The latter approach is the basis of TPM and its variants, which afford an entire core-level spectrum

*herbert@chemistry.ohio-state.edu

(at one particular edge) from a single calculation.[18] These methods have the same computational cost as a single "ΔSCF" calculation (Section 2 A) but without the need for state-by-state calculations and with less concern about variational collapse. They may hold some advantages for modeling complex systems or experiments, insofar as the spectrum is computed in a single shot and is closely tied to Kohn-Sham eigenvalue information (chemical shifts).

Like the ΔSCF approach, however, eigenvalue-based methods may depend sensitively on the choice of exchange-correlation (XC) functional. The present work systematically investigates different approaches using XC functionals on various rungs of Jacob's ladder.[21] It follows a similar investigation of fractional-electron methods for computing core-level electron binding energies,[44] as in x-ray photoelectron spectroscopy (XPS). In that previous work, we demonstrated that an empirically-shifted version of STM with a single fitting parameter affords K-shell electron binding energies that are more accurate than those obtained from the best *ab initio* methods, including *GW*-type methods.[44] A similar empirical shifting procedure is introduced here, for core-to-valence excitation energies.

2 Theoretical Methods

This section introduces eigenvalue-based methods for computing core-to-valence excitation energies based on a time-independent, ground-state DFT formalism. Conceptually, these methods are approximations to a ΔSCF calculation, which we therefore consider first.

A. ΔSCF Method. The ΔSCF approach for excitation energies has also been called "excited-state Kohn-Sham theory",[21,25] as it is based on finding a non-*Aufbau* Slater determinant to represent an excited state. The excitation energy is then simply the energy difference,

$$\Delta E = E_\mathrm{f} - E_\mathrm{i} \;, \tag{3}$$

where E_i and E_f are the total energies of the ground-state determinant and the non-*Aufbau* determinant, respectively, the latter of which contains a core hole. Various algorithms have been developed to relax the MOs for a non-*Aufbau* determinant while avoiding variational collapse to the ground state or other lower-lying state.[68–73] The maximum overlap method (MOM)[69–71] often works well for the lowest excited state (or the lowest state of a given symmetry), and has previously been applied to core-to-LUMO excitations.[74] In our experience, however, more sophisticated methods are often required to converge higher-lying excited states.[73]

B. Slater-Type Methods. The use of fractional-electron SCF calculations originated with Slater,[52–54] although these are now used widely as a means to diagnose and correct problems with delocalization error and self-interaction in DFT.[59,75–83] Fractional-electron calculations have also been used in conjunction with correlated wave function models.[84–87]

Slater's original transition method,[52–54] formulated here for a core → virtual ($c \to \upsilon$) excitation, is based on promoting $n_c = 1/2$ electron into a valence virtual MO, so that $n_\upsilon = 1/2$. To understand why this is relevant, imagine the energy $E(\{n_i\})$ of a Slater determinant is expanded as a Taylor series in orbital occupation numbers $\{n_i\}$, treated as continuous variables. Setting $E_0 = E(\{n_i^0\})$, one may write

$$E = E_0 + \sum_i (n_i - n_i^0)\varepsilon_i + \frac{1}{2}\sum_{i,j}(n_i - n_i^0)(n_j - n_j^0)\frac{\partial^2 E}{\partial n_i \partial n_j} + \cdots \tag{4}$$

where we have used the Slater-Janak theorem,[88] $\varepsilon_i = \partial E/\partial n_i$. We wish to approximate the ΔSCF excitation energy in eq. 3, which we write as

$$\Delta E = E(0,1) - E(1,0) \tag{5}$$

where $E_\mathrm{i} = E(1,0)$ and $E_\mathrm{f} = E(0,1)$ are the initial and final state energies, expressed in the form $E(n_c, n_\upsilon)$. Choosing the reference state $\{n_i^0\}$ in eq. 4 to be $n_c = 1/2 = n_\upsilon$, one obtains a leading-order approximation $\Delta E \approx \Delta E_\mathrm{STM}$, where[21,53]

$$\Delta E_\mathrm{STM} = \varepsilon_\upsilon(1/2, 1/2) - \varepsilon_c(1/2, 1/2) \;. \tag{6}$$

In this and subsequent equations, we use the notation $\varepsilon_r(n_c, n_\upsilon)$ to mean the Kohn-Sham eigenvalue for MO ψ_r, obtained from an SCF calculation that employs occupancies n_c and n_υ for the core and virtual orbitals in question. (We assume spin-orbitals in this notation, so $0 < n_c \leq 1$ and $0 \leq n_\upsilon \leq 1$, and all calculations are performed within a spin-unrestricted formalism.) Alternative derivations of eq. 6 have also been suggested,[21,58,59] *e.g.*, based on integration of $\partial E/\partial n_r$ starting from a determinant with integer occupancies,[58] or based on cancellation of self-interaction error.[59]

Although formulated above for $c \to \upsilon$ excitation, the STM has also been used to estimate core-electron binding energies (CEBEs),[44,83,89–92] via a Koopmans-style approximation but with a fractional occupancy ($n_c = 1/2$) for the core level in question. Using a notation similar to that introduced above, this approximation is

$$\mathrm{CEBE}_c \approx -\varepsilon_c(1/2) \;. \tag{7}$$

(Variants with $n_c = 2/3$ or $n_c = 3/4$ have also been suggested.[44,59]) In a recent study of K-shell CEBEs,[44] we found that eq. 7 affords an accuracy of ∼ 0.5 eV at the Hartree-Fock level but is significantly less accurate at DFT levels of theory. Reasonable accuracy was recovered (even for DFT) using generalized approaches that

require more than one fractional-electron SCF calculation per CEBE.[44,59,60] Similar ideas for excitation energies are explored below.

The simple STM in eq 6 overestimates excitation energies.[44] This observation motivated a generalization in which the fractional-electron SCF calculation is mixed with a ground-state eigenvalue difference,[58] a method that can be understood as a higher-order extension of Slater's original transition method.[58,89] For excitation energies, this generalized (G)STM takes the form

$$\Delta E_{\mathrm{GSTM}} = \frac{1}{4}\big[\varepsilon_v(1,0) + 3\varepsilon_v(1/3,2/3) - \varepsilon_c(1,0) - 3\varepsilon_c(1/3,2/3)\big] \; . \tag{8}$$

Here, $\varepsilon_c(1,0)$ and $\varepsilon_v(1,0)$ are eigenvalues from a ground-state calculation ($n_c = 1$ and $n_v = 0$), whereas $\varepsilon_v(1/3,2/3)$ and $\varepsilon_c(1/3,2/3)$ come from a fractional-occupancy calculation with $n_c = 1/3$ and $n_v = 2/3$. In the early days of molecular DFT calculations, the GSTM approach showed promising accuracy of ~ 0.3 eV for K-shell electron binding energies,[89–91] although this was later shown to benefit from some error cancellation.[92] Other schemes involving different fractional occupancies have been proposed more recently,[44,59,60] and we have elsewhere evaluated some of them for CEBEs.[44]

C. Transition Potential Methods. As originally formulated (to approximate a ΔSCF calculation), the STM and its generalizations require separate SCF calculations for each excited state of interest, *i.e.*, for each virtual level ε_v into which a fractional electron is promoted. Like the ΔSCF approach itself, this is a tedious and inconvenient way to compute an entire spectrum, and promotions beyond the LUMO are prone to variational collapse in the absence of symmetry constraints. Alternatives are to modify the core occupancy only, leaving the virtual space empty ($n_v = 0$), or else to promote an electron or fraction of an electron into the LUMO, then use the full spectrum of virtual eigenvalues to estimate excitation energies ($\Delta E = \varepsilon_v - \varepsilon_c$). The latter approximation assumes that the potential generated by the LUMO is similar to that generated by the higher-lying virtual orbitals.

The widely-used TPM[18,51,61–63] corresponds to the first of these alternative strategies, in which no electrons whatsoever are placed in the virtual space. Excitation energies within the TPM are given by

$$\Delta E_{\mathrm{TPM}} = \varepsilon_v(1/2,0) - \varepsilon_c(1/2,0) \; . \tag{9}$$

For obvious reasons, this method has also been called the "half core-hole" (HCH) approach.[93] A generalized (G)TPM can then be envisioned in the spirit of eq 8:

$$\Delta E_{\mathrm{GTPM}} = \frac{1}{4}\big[\varepsilon_v(1,0) + 3\varepsilon_v(1/3,0) - \varepsilon_c(1,0) - 3\varepsilon_c(1/3,0)\big] \; . \tag{10}$$

Note that $n_c + n_v \neq 1$ for the fractional-occupation calculation that is used to obtain $\varepsilon_v(1/3,0)$ and $\varepsilon_c(1/3,0)$, so that calculation involves a charged system. This can be a problem for DFT under periodic boundary conditions,[18,94] therefore some charge-neutral alternatives have been explored.[51,64] These are discussed below.

A summary of different approximations is provided in Table 1, in the form

$$\Delta E = F_v - F_c \tag{11}$$

where F_v and F_c are simple functions of ε_v and ε_c, respectively, computed from one or more SCF calculations that typically involve fractional occupancies and a (fractional) core hole. In addition to methods discussed above, the list in Table 1 also includes the FCHM approach,[18,65–67] which is the $n_c = 0$ analogue of the TPM/HCH method in eq 9. In FCHM, a full electron is removed from the core but nothing is placed in the virtual space:

$$\Delta E_{\mathrm{FCHM}} = \varepsilon_v(0,0) - \varepsilon_c(0,0) \; . \tag{12}$$

As with the TPM and GTPM methods, this procedure creates a charged system. A charge-neutral alternative is the extended core-hole method (XCHM),[51] in which an entire electron is removed from the core and placed in the LUMO:

$$\Delta E_{\mathrm{XCHM}} = \varepsilon_v(0,1) - \varepsilon_c(0,1) \; . \tag{13}$$

D. Excitation Beyond the LUMO. Eigenvalue-based methods can be extended to higher-lying transitions, but such calculations often suffer variational collapse or other SCF convergence issues if a electron (or a fraction of an electron) must be promoted into a virtual orbital above the LUMO. Transition-potential approaches sidestep this problem by using the LUMO's potential to stand in for that of higher-lying virtual orbitals, and an especially promising protocol is the charge-neutral XCHM procedure.[51] Generalizing eq 13 for virtual orbitals v lying beyond the LUMO, we have

$$\Delta E_{\mathrm{XCHM}} = \varepsilon_v(0, n_{\mathrm{LUMO}} = 1) - \varepsilon_c(0, n_{\mathrm{LUMO}} = 1) \; . \tag{14}$$

Recently, charge-neutral variants of TPM and GTPM have been suggested,[18,51] called the extended (X)TPM and the extended (X)GTPM, respectively. These methods correspond to the formulas

$$\Delta E_{\mathrm{XTPM}} = \varepsilon_v(1/2, n_{\mathrm{LUMO}} = 1/2) - \varepsilon_c(1/2, n_{\mathrm{LUMO}} = 1/2) \tag{15}$$

and

$$\Delta E_{\mathrm{XGTPM}} = \frac{1}{4}\big[\varepsilon_v(1, n_{\mathrm{LUMO}} = 0) + 3\varepsilon_v(1/3, n_{\mathrm{LUMO}} = 2/3) - \varepsilon_c(1, n_{\mathrm{LUMO}} = 0) - 3\varepsilon_c(1/3, n_{\mathrm{LUMO}} = 2/3)\big] \; . \tag{16}$$

Table 1: Eigenvalue-Based Approximations for Core-to-Valence Excitation Energies[a]

Method	F_υ	F_c	Occupancies
STM	$\varepsilon_\upsilon(n_c, 1-n_c)$	$\varepsilon_c(n_c, 1-n_c)$	$n_c = 1/2$
GSTM[b]	$[\varepsilon_\upsilon(n_c, 1-n_c) + 3\varepsilon_\upsilon(n_c', 1-n_c')]/4$	$[\varepsilon_c(n_c, 1-n_c) + 3\varepsilon_c(n_c', 1-n_c')]/4$	$n_c = 1, n_c' = 1/3$
TPM	$\varepsilon_\upsilon(n_c, n_\upsilon)$	$\varepsilon_c(n_c, n_\upsilon)$	$n_c = 1/2, n_\upsilon = 0$
GTPM	$[\varepsilon_\upsilon(n_c, n_\upsilon) + 3\varepsilon_\upsilon(n_c', n_\upsilon)]/4$	$[\varepsilon_c(n_c, n_\upsilon) + 3\varepsilon_c(n_c', n_\upsilon)]/4$	$n_c = 1, n_\upsilon = 0,$ $n_c' = 1/3$
FCHM	$\varepsilon_\upsilon(n_c, n_\upsilon)$	$\varepsilon_c(n_c, n_\upsilon)$	$n_c = 0 = n_\upsilon$
XCHM	$\varepsilon_\upsilon(n_c, 1-n_c)$	$\varepsilon_c(n_c, 1-n_c)$	$n_c = 0$
XTPM	$\varepsilon_\upsilon(n_c, n_{\mathrm{LUMO}} = 1-n_c)$	$\varepsilon_c(n_c, n_{\mathrm{LUMO}} = 1-n_c)$	$n_c = 1/2$
XGTPM[b]	$[\varepsilon_\upsilon(n_c, n_{\mathrm{LUMO}} = 1-n_c) + 3\varepsilon_\upsilon(n_c', n_{\mathrm{LUMO}}' = 1-n_c')]/4$	$[\varepsilon_c(n_c, n_{\mathrm{LUMO}} = 1-n_c) + 3\varepsilon_c(n_c', n_{\mathrm{LUMO}}' = 1-n_c')]/4$	$n_c = 1, n_c' = 1/3$

[a] $\Delta E = F_\upsilon - F_c$ (eq 11). [b] These methods require two SCF calculations.

Lastly, we consider the ionization potential-corrected TPM method (IP-TPM).[18,61] This approach removes $n_c = 1/2$ from the core and uses the formula

$$\Delta E_{\text{IP-TPM@1/2}} = \varepsilon_\upsilon(1/2, 0) + \Delta E_{\text{IP}} \tag{17}$$

for the transition energies, where ΔE_{IP} is the absolute CEBE for the occupied orbital in question, computed using a ΔSCF approach. We will also consider an alternative formulation with $n_c = 1/3$:

$$\Delta E_{\text{IP-TPM@1/3}} = \varepsilon_\upsilon(1/3, 0) + \Delta E_{\text{IP}} \ . \tag{18}$$

Physically, both of these methods include the core-hole relaxation effects in valence states, which is important for relative peak positions and intensities, while ΔE_{IP} helps to incorporate core-hole screening and thus to provide reliable chemical shifts.[18] Both IP-TPM approaches can be used for core → LUMO and higher-lying excitations.

E. Limitations. Slater-style methods are intended as extremely simple approaches for excitation or ionization energy calculations that exploit only the information contained in ground-state Kohn-Sham eigenvalues, albeit possibly for a fictitious fractional-electron ground state. The simplicity of this approach may hold advantages for complex systems but also imbues these methods with significant limitations, some of which are worth pointing out. First of all, these methods do not include spin coupling so there is no distinction between singlet and triplet excitations starting from a singlet ground state. The singlet–triplet excitation gap for $c \to \upsilon$ excitation could be estimated as[95,96]

$$E_{\text{singlet}} - E_{\text{triplet}} \approx 2\big[(c\upsilon|c\upsilon) - (cc|\upsilon\upsilon)\big] \ . \tag{19}$$

If one is willing to introduce two-electron integrals, then one may also correct the ΔSCF result via perturbation theory.[97–101] However, direct use of electron repulsion integrals is a step away from the purpose of using eigenvalue-based methods in the first place. As such, we will not attempt to compute any spin couplings in the present work.

A separate issue is that these methods might exhibit a state-assignment problem in certain cases, insofar as the identification of excited states is explicitly tied to (and therefore cannot go beyond) the MO picture. Limitations of the MO picture for both excitation[95,96,102] and ionization,[103] due to electron correlation effects, have been discussed elsewhere. In the context of ΔSCF calculations of core-excited states, this is sometimes discussed in terms of the missing "many-electron response to the core hole".[104] When using the methods described herein, that response is taken into account (if at all) merely in terms of the fractional nature of the core hole.

3 Computational Details

Fractional-occupancy methods have been implemented in a locally-modified version of Q-Chem,[105] and will be made available in v. 6.1. Although various algorithms are available to optimize a non-*Aufbau* determinant that contains a fractional core hole,[69–73] the calculations presented herein use either the MOM algorithm[69] or else the "initial MOM" (IMOM) algorithm.[70] These differ only in whether overlaps are computed with respect to the previous SCF cycle's occupied MOs (in the MOM procedure), or else with respect the MOs at the first SCF cycle (in IMOM).

Density functionals examined here include SCAN,[106] SCAN0 (having 25% exact exchange),[107] B3LYP,[108,109] ωB97X-V,[110] Becke's "half-and-half" functional (BH&HLYP) with 50% exact exchange, and CAM-B3LYP,[111] where the range-separation parameter is $\omega = 0.33$ bohr^{-1}. We also examine the long-range corrected (LRC) functionals LRC-

ωPBE (with $\omega = 0.3$ bohr^{-1}) and LRC-ωPBEh ($\omega = 0.2$ bohr^{-1}).[112–114] Relative to LRC-ωPBE, note that LRC-ωPBEh includes 20% exact exchange at short range.[114] The SRC1-r1 functional,[40] which was parameterized for K-edge transition energies using TD-DFT and performs well in that capacity,[40,41,115] affords extremely large errors in ΔSCF calculations; see Tables S1 and S2. Similarly poor performance for this functional is observed in ΔSCF calculations of CEBEs,[44] and therefore SRC1-r1 is not considered further.

The def2-QZVPD basis set is used for all calculations, in an effort to separate basis-set errors from methodological errors. Previous results for CEBEs indicate that DFT/def2-QZVP values are converged, such that uncontracting the core functions makes negligible difference,[44] whereas uncontracting the basis set changes DFT/def2-TZVP binding energies by ~ 0.4 eV.[44] We add a set of diffuse functions here, in order to better describe the virtual orbitals. Mean absolute errors (MAEs) for ΔSCF calculations using SCAN, SCAN0, and B3LYP are 0.3 eV for 1s → LUMO excitation, whereas K-shell ΔSCF ionization energy errors with these same functionals are 0.2–0.3 eV.[44] Addition of a second set of diffuse functions to def2-QZVPD reduces the MAE from 0.31 eV to 0.25 eV (see Table S3), for a data set that includes excitations beyond the LUMO, and excitation energy differences between the two basis sets are < 0.2 eV, on average. As such, we regard that the present results are well converged.

For XC functionals that are generalized gradient approximations (GGAs) or hybrids thereof, we use the SG-1 quadrature grid.[116] The SG-3 grid[117] is used for meta-GGA functionals and their hybrids. However, tests using the smaller SG-2 grid[117] showed no differences, even for functionals such as SCAN with well-documented grid sensitivity.[118] This suggests that SG-2 would have been sufficient for the calculations reported here.

All calculations are performed using a spin-unrestricted formalism. We apply Boys localization[119] prior to the fractional-electron or other non-*Aufbau* SCF calculation (including ΔSCF), in order to avoid problems in cases where symmetry-equivalent atoms give rise to delocalized core orbitals. This issue is not unique to DFT calculations,[120–123] and a detailed analysis suggests that orbital relaxation and electron correlation effects are comparable in magnitude for ionization from a delocalized core state, whereas relaxation effects dominate when localized orbitals are used.[121] This explains the success of the ΔSCF approach with low-level electron correlation methods (or with no correlation at all), and argues for the use of a localized initial state even in the presence of symmetry-equivalent atoms.[18,122–126] Although Boys localization was used for all calculations reported here, spot checks suggest that its effect is practically nil for the examples that we consider, even for a molecule like ethylene with symmetry-equivalent C(1s) orbitals. The effect of localization is somewhat larger for CEBEs.

Element-specific relativistic corrections have been included in all theoretical results, as in previous work,[44] so that they may be compared directly to experiment. These corrections were taken from Ref. 127 and they are 0.14 eV for C(1s), 0.28 eV for N(1s), 0.51 eV for O(1s), and 0.85 eV for F(1s), which are close to values reported elsewhere.[36] These corrections are added to the non-relativistic excitation energy, meaning that the corrected excitation energy is larger than the non-relativistic result, *e.g.*, by 0.14 eV for carbon K-edge excitation energies.

4 Results and Discussion

We survey the methods introduced above as applied to 1s → LUMO transitions, in Section 4 A, as well as higher-lying transitions (1s → LUMO+1, LUMO+2, ...) in Section 4 B. Statistical assessments in terms of MAEs are given here but all computational results can be found in the Supporting Information. An empirically-shifted approach is presented in Section 4 C, and finally we consider full XAS spectra (including oscillator strengths) in Section 4 D.

A. K-Edge Transitions. Table 2 reports MAEs versus experiment for a data set of 1s → LUMO transitions that is taken from Ref. 128. These data consist of excitation energies at the elemental K-edge for carbon (14 data points), nitrogen (8 data points), oxygen (11 data points), and fluorine (4 data points).

When only the elemental K-edge (and not any higher-lying states) is desired, the ΔSCF procedure is usually straightforward and ΔSCF results therefore serve as a baseline (for a given XC functional) to evaluate alternative Slater-style methods based on Kohn-Sham eigenvalues. At the ΔSCF level, several functionals afford results within ~ 0.3 eV of experiment when atomic relativistic corrections are included: SCAN, SCAN0, and B3LYP. The functionals BH&HLYP, CAM-B3LYP, and ωB97X-V afford MAEs that are slightly larger but still below 0.5 eV. These errors are comparable to statistical errors in K-shell ionization energies for the same functionals.[44] Whereas an early study[129] suggested that ΔSCF calculations of core-level excitation energies might be significantly more accurate than those for core ionization (due to error cancelation involving the core hole in the former case), that conclusion is not borne out for the present data set and functionals.

The LRC-ωPBE and LRC-ωPBEh functionals do not fare particularly well at the ΔSCF level yet afford the smallest MAEs for the STM approach, whereas STM errors for other functionals lie in the range 1–2 eV. Note that LRC functionals have been used in the past to improve the agreement between valence Kohn-Sham energy levels and ionization energies,[79,130,131] but these functionals are inferior to B3LYP for K-edge excitation en-

Table 2: Error Statistics (Versus Experiment) for 1s → LUMO Transitions.[a]

Method	Core Orbital	Mean Absolute Error (eV)[b]							
		SCAN	SCAN0	B3LYP	BH&HLYP	CAM-B3LYP	LRC-ωPBE	LRC-ωPBEh	ωB97X-V
ΔSCF	all	0.33	**0.29**	**0.29**	0.43	0.36	1.10	0.82	0.41
ΔSCF	C(1s)	0.51	0.43	0.42	**0.39**	0.49	1.35	1.02	0.33
ΔSCF	N(1s)	0.26	**0.22**	0.29	0.43	0.31	1.03	0.70	0.41
ΔSCF	O(1s)	0.14	0.17	0.19	0.34	0.21	0.98	0.74	0.39
ΔSCF	F(1s)	0.38	0.25	**0.08**	0.80	0.39	0.64	0.53	0.72
STM[c]	all	2.43	1.86	1.03	1.16	1.18	**0.85**	0.88	1.87
STM[c]	C(1s)	1.82	1.45	0.79	0.85	0.80	**0.50**	0.57	1.53
STM[c]	N(1s)	2.47	1.97	1.02	1.33	1.22	**0.89**	**0.89**	1.89
STM[c]	O(1s)	2.82	2.05	1.18	1.26	1.37	**1.01**	1.10	2.08
STM[c]	F(1s)	3.43	2.50	1.44	1.65	1.94	1.51	**1.32**	2.43
GSTM	all	0.90	0.68	**0.30**	0.53	0.40	0.53	0.42	0.73
GSTM	C1s	0.54	0.43	**0.33**	0.40	0.38	0.78	0.64	0.62
GSTM	N1s	0.77	0.68	**0.14**	0.72	0.43	0.53	0.47	0.77
GSTM	O1s	1.18	0.83	0.28	0.47	0.32	0.37	**0.25**	0.75
GSTM	F1s	1.67	1.13	0.61	0.74	0.68	0.07	**0.04**	0.99
TPM	all	3.84	4.26	**2.92**	4.34	4.44	4.83	4.55	6.02
TPM	C1s	3.50	4.22	**2.86**	4.40	4.32	4.59	4.49	5.91
TPM	N1s	3.64	3.49	**2.77**	4.21	4.25	4.72	4.02	5.85
TPM	O1s	4.11	4.58	**2.99**	4.23	4.55	5.05	4.88	6.13
TPM	F1s	4.72	5.07	**3.22**	4.74	4.95	5.29	4.92	6.46
GTPM	all	2.23	2.96	**2.13**	4.06	3.26	3.56	3.38	4.61
GTPM	C1s	2.13	2.77	**2.02**	4.33	3.12	3.41	3.22	4.57
GTPM	N1s	**1.98**	2.85	1.95	3.99	2.98	2.94	3.34	4.34
GTPM	O1s	**2.32**	3.04	2.33	3.60	3.39	4.03	3.43	4.55
GTPM	F1s	2.85	3.64	**2.29**	4.50	3.97	3.99	3.85	5.40
FCHM	all	2.38	**2.33**	5.85	1.84	5.46	7.74	3.45	6.47
FCHM	C1s	1.31	2.27	4.64	**1.11**	4.23	5.21	2.19	4.95
FCHM	N1s	**1.80**	2.49	5.45	2.30	4.94	7.14	3.01	5.99
FCHM	O1s	3.09	2.50	6.56	**2.42**	6.21	9.50	4.23	7.46
FCHM	F1s	5.38	**1.75**	8.90	1.86	8.72	12.95	6.61	10.07
XCHM	all	**1.65**	6.77	2.51	7.15	2.24	2.88	4.04	2.74
XCHM	C1s	**1.65**	7.14	1.07	6.59	3.07	3.38	5.94	4.24
XCHM	N1s	**1.03**	7.03	1.94	7.29	1.96	2.12	3.79	2.11
XCHM	O1s	1.27	6.55	3.51	8.10	**1.08**	1.91	2.74	1.31
XCHM	F1s	3.87	5.55	5.94	6.23	3.12	5.33	**1.43**	2.72
IP-TPM@1/2	all	**1.20**	2.16	1.68	3.58	3.10	2.97	3.02	4.58
IP-TPM@1/2	C1s	**1.16**	2.03	1.85	3.68	3.13	2.98	3.03	4.60
IP-TPM@1/2	N1s	**1.04**	1.95	1.54	3.45	2.94	2.84	2.95	4.40
IP-TPM@1/2	O1s	**1.23**	2.26	1.52	3.37	3.04	2.95	2.96	4.54
IP-TPM@1/2	F1s	**1.59**	2.74	1.82	4.06	3.50	3.24	3.27	4.97
IP-TPM@1/3	all	0.72	0.82	**0.39**	1.89	1.52	1.37	1.43	3.03
IP-TPM@1/3	C1s	0.72	0.94	**0.60**	2.06	1.52	1.32	1.41	3.01
IP-TPM@1/3	N1s	0.67	0.72	**0.16**	1.50	1.44	1.36	1.46	2.97
IP-TPM@1/3	O1s	0.69	0.69	**0.26**	1.80	1.49	1.40	1.41	3.01
IP-TPM@1/3	F1s	0.89	0.99	**0.44**	2.29	1.76	1.49	1.52	3.27

[a]Data set consists of 37 K-edge transitions from Ref. 128 and all theoretical values include an atomic relativistic correction. [b]The smallest MAE in each row is presented in boldface and the largest is underlined. [c]For core → LUMO excitation, STM is equivalent to XTPM.

ergies in TD-DFT.[132] The performance might be improved via "optimal tuning",[133] adjusting ω such that $\varepsilon_{\mathrm{HOMO}} = -\Delta E_{\mathrm{IP}}$, but we have not pursued this strategy, in the interest of obtaining a black-box method that does not need to be adjusted for each new molecule. (Optimally-tuned values of ω are often strongly dependent on system size, even for a sequence of homologous systems.[134–137])

In previous work on CEBEs, we showed that STM is not competitive with ΔSCF but that some variants of GSTM approach the accuracy of ΔSCF.[44] This can be understood based on the fact that GSTM amounts to a higher-order Taylor series approximation,[89] a higher-order quadrature scheme (for a type of thermodynamic integration),[58] or as more effective cancellation of self-interaction error.[59] The same is true for these K-edge excitations, where all functionals tested afford MAEs smaller than 1 eV at the GSTM level. Using B3LYP,

the GSTM and ΔSCF results are quite similar.

We next consider the transition-potential approaches: TPM (eq 9) and GTPM (eq 10). These methods modify only the core occupancy n_c and do not put any electrons into the virtual space, resulting in underestimation of the electron–hole attraction and thus a shift to higher excitation energies.[18] This is evident in the data presented in Table 2, where GTPM errors are generally smaller than TPM errors yet even the former are larger than 2 eV for all functionals tested. FCHM (eq 12), which also does not place electrons into the virtual space, affords similarly large errors. Given that these methods also create a charged system, and are therefore problematic under periodic boundary conditions, neither TPM, GTPM, nor FCHM can be recommended. Nevertheless, these continue to be widely-used methods.[67,94,138–142] Results for relative peak positions in near-edge XAS spectra are better than absolute excitation energy predictions.[51]

The XCHM approach (eq 13) creates a charge-neutral excitation but we find that results are erratic, improving somewhat with respect to TPM-style methods for certain functionals (*e.g.*, SCAN and CAM-B3LYP) yet seriously degraded as compared to TPM approaches when some other functionals are used, such as BH&HLYP for which the XCHM error exceeds 7 eV. The XCHM also continues to enjoy widespread use in materials science and other condensed-phase applications,[142–150] despite its wild sensitivity with respect to the choice of XC functional.

Finally, the performance of IP-TPM@1/2 and IP-TPM@1/3 is quite interesting. For a given functional, these methods typically afford smaller errors as compared to any of the TPM-based approaches that do not place electrons in the virtual space, and they also perform better than XCHM in many cases. IP-TPM@1/3 is consistently better than other eigenvalue-based approaches, affording MAEs below 1 eV when used in conjunction with SCAN, SCAN0, or B3LYP. For B3LYP the MAE is 0.3 eV when using IP-TPM@1/3, essentially identical to the statistical error in ΔSCF results for the same functional.

B. Higher-Lying Near-Edge Transitions. Table 3 reports error statistics for a data set of 20 higher-lying, dipole-allowed transitions originating from C(1s) orbitals (8 transitions), N(1s) orbitals (6 transitions), and O(1s) orbitals (6 transitions). These are "higher-lying" transitions in the sense that the final state is not the LUMO. Experimental excitation energies are taken from various sources as detailed in the Supporting Information. For each of the methods except ΔSCF, the full XAS spectrum is evaluated by populating the LUMO (only) with a fractional electron. As discussed above, this makes the eigenvalue-based methods more robust against variational collapse, as compared to the ΔSCF procedure that does involve excitation beyond the LUMO.

The accuracy for these higher-lying transitions is not as good as what we reported for 1s → LUMO transitions, and this conclusion holds across a variety of XC functionals. For the best-performing functionals (SCAN, SCAN0, and B3LYP), the accuracy of the ΔSCF procedure is only slightly worse than it was for the 1s → LUMO transitions, and MAEs are smaller than 0.5 eV even for the higher-lying transitions, although (perhaps surprisingly) the ωB97X-V functional exhibits a MAE of 1.2 eV for this data set, as compared to 0.4 eV for the K-edge transitions.

It has been noted that transition-potential methods do not exhibit the correct asymptotic electron–ion potential for high-lying Rydberg states,[151] which may place some limitations on the accuracy of higher-lying excitation energies. Regarding the eigenvalue-based approaches examined here, the widely-used XCHM affords MAEs larger than 1 eV for every functional that we tested, including very large MAEs of 5.0 eV for XCHM-SCAN0 and 2.8 eV for XCHM-B3LYP. XGTPM is the best-performing eigenvalue method, with MAEs of 0.7–0.8 eV when used with either SCAN, SCAN0, or B3LYP. To reduce these errors, we turn to an empirical shifting scheme that proved quite successful for core-level electron binding energies.[44]

C. Empirically-Shifted Method. In previous work,[44] we demonstrated that introduction of a single, functional-specific shifting parameter turned the primitive STM approach into the most accurate electronic structure method for K-shell CEBEs, outperforming not only ΔSCF calculations but also more expensive methods including variants of the *GW* approach. In a similar spirit, we introduce an empirically-shifted version of XTPM,

$$\Delta E^{\text{shifted}}_{\text{XTPM}} = \Delta E_{\text{XTPM}} + \delta_v \; . \tag{20}$$

Here, ΔE_{XTPM} is the XTPM excitation energy defined in eq 15, and the shift δ_v is given by

$$\begin{aligned}\delta_v = \beta\big[&\varepsilon_c(1,0) - \varepsilon_c(1/2, n_{\text{LUMO}} = 1/2) \\ &- \varepsilon_v(1,0) + \varepsilon_v(1/2, n_{\text{LUMO}} = 1/2)\big]\end{aligned} \tag{21}$$

where β is an empirical parameter. The shift corrects for excitation energies that are overestimated by XTPM. Note that eqs. 20 and 21 can be rewritten in the form

$$\Delta E^{\text{shifted}}_{\text{XTPM}} = (1+\beta)\Delta E_{\text{XTPM}} - \beta\big[\varepsilon_v(1,0) - \varepsilon_c(1,0)\big] \; , \tag{22}$$

which demonstrates that the shifted XTPM approach can also be viewed as a weighted average of the original XTPM excitation energy (ΔE_{XTPM}) and the unrelaxed orbital energy difference, $\varepsilon_v(1,0) - \varepsilon_c(1,0)$.

Unlike the shifted-STM approach for CEBEs that was introduced in Ref. 44, for excitation energies the shift δ_v depends on the virtual MO ψ_v, even for a given x-ray edge (corresponding to a given occupied MO, ψ_c). To determine β, we use the same data set of 20 higher-lying excitation energies used to obtain the error statistics in

Table 3: Error Statistics (Versus Experiment) for Higher-Lying K-Edge Transitions.[a]

Method	Mean Absolute Error (eV)[b]							
	SCAN	SCAN0	B3LYP	BH&HLYP	CAM-B3LYP	LRC-ωPBE	LRC-ωPBEh	ωB97X-V
ΔSCF	0.35	0.48	**0.31**	0.98	0.45	0.67	0.35	1.23
XCHM	**1.14**	5.00	2.78	5.26	1.87	3.58	1.59	2.98
XTPM	2.05	1.57	**0.68**	1.54	1.23	1.73	1.31	2.43
XGTPM	**0.68**	**0.68**	0.79	1.32	0.92	1.47	0.92	1.55
IP-TPM@1/2	2.52	2.60	**1.93**	3.09	2.72	2.60	2.64	3.82
IP-TPM@1/3	1.48	1.65	**0.90**	2.12	1.75	1.86	1.70	2.90

[a]Data set consists of 20 transitions from C(1s), N(1s), and O(1s) orbitals and all theoretical values include an atomic relativistic correction. [b]The smallest MAE in each row is presented in boldface and the largest is underlined.

Table 4: Errors for Higher-Lying K-Edge Transitions,[a] Using the Shifted-XTPM Approach (eq 20).

Functional	β	MAE (eV)
SCAN	4.0	0.63
SCAN0	6.0	0.73
B3LYP	1.5	0.66
BH&HLYP	−8.0	1.61
CAM-B3LYP	3.0	0.68
LRC-ωPBE	2.0	1.26
LRC-ωPBEh	3.5	0.75
ωB97X-V	6.0	0.72

[a]Same data set as in Table 3, def2-QZVPD basis set.

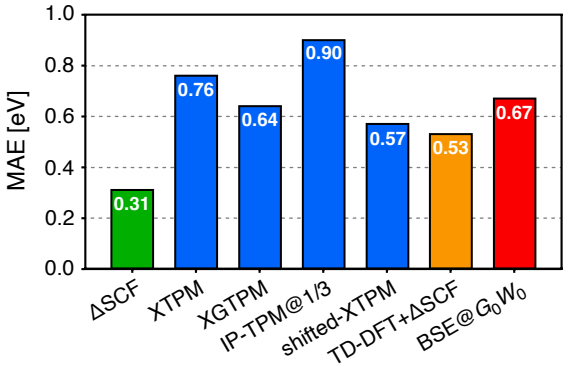

Fig. 1: MAEs for a data set of 29 C(1s), N(1s), and O(1s) core-to-valence excitation energies, using various approaches. Methods in blue are eigenvalue-based approaches. All calculations use the B3LYP functional except for the BSE@G_0W_0 values, which are taken from Ref. 36 and use LRC-ωPBEh. The TD-DFT+ΔSCF results are from Ref. 23, where a ΔSCF calculation of the 1s $\rightarrow$ LUMO excitation energy is used to shift the spectrum from a TD-DFT calculation. Numerical values of the MAE (in eV) are shown for each entry.

Table 3. Fitted values of β for several different XC functionals are listed in Table 4 along with MAEs for the corresponding shifted-XTPM approach defined by eq. 20. (The best-fit values do have some basis-set sensitivity.)

For most of the XC functionals considered here, this empirical shift considerably improves the accuracy of the XTPM approach, although BH&HLYP and B3LYP, and LRC-ωPBE are exceptions that show little improvement. MAEs of 0.6–0.7 eV are obtained from shifted XTPM calculations using any of the functionals SCAN, SCAN0, B3LYP, or CAM-B3LYP.

To put this level of accuracy in context alongside other state-of-the-art approaches, Fig. 1 illustrates the errors alongside some of the competing alternatives. The data set consists of 29 K-edge and near-edge excitation energies for which BSE@G_0W_0 results are available,[36] and the latter method is compared to ΔSCF and also to four different eigenvalue-based methods, using the B3LYP functional for all but the BSE@G_0W_0 calculations. We also juxtapose results in which a TD-DFT excitation spectrum is shifted so that its lowest excitation energy matches the 1s $\rightarrow$ LUMO excitation energy from a ΔSCF calculation.[23] This shift serves to eliminate what are otherwise rather large[38–43] (but systematic[152]) errors in TD-DFT excitation energies.

Several alternative methods are able to match or outperform BSE@G_0W_0, for which the MAE is 0.67 eV.[36] Even without empirical shifting, the eigenvalue-based XTPM performs almost as well (MAE = 0.76 eV), and even better with empirical shifting (MAE = 0.57 eV), while XGTPM performs about as well as BSE@G_0W_0 (MAE = 0.64 eV). The accuracy of both methods is comparable to that of TD-DFT with a ΔSCF shift (MAE = 0.53 eV).[23] The ΔSCF approach remains the most accurate (even as compared to BSE@G_0W_0), with a MAE of 0.31 eV, but requires a separate calculation for each state.

Finally, we examine the performance of the shifted-XTPM approach for 1s $\rightarrow$ LUMO excitations that were not included in the training set that was used to determine the β parameter. For this, we use the same data set as in Table 2, with results summarized in Table 5 for a variety of XC functionals. The empirical shift significantly narrows the accuracy gap between different functionals, all of which afford overall errors smaller than 1 eV. Importantly, for SCAN, B3LYP, and CAM-B3LYP the MAEs are $\lesssim$ 0.7 eV even when the higher-lying transitions are considered. Shifted-XTPM using SCAN or B3LYP is therefore recommended for full-spectrum XAS

Table 5: Error Statistics (Versus Experiment) for 1s → LUMO Transitions Using Shifted-XTPM.[a]

Core Orbital	Mean Absolute Error (eV)[b]							
	SCAN	SCAN0	B3LYP	BH&HLYP	CAM-B3LYP	LRC-ωPBE	LRC-ωPBEh	ωB97X-V
all	**0.29**	0.64	0.51	0.85	0.35	0.47	0.41	0.50
C(1s)	**0.35**	0.70	0.45	0.50	0.38	0.54	0.44	0.58
N(1s)	**0.27**	0.54	0.55	1.11	0.40	0.39	0.30	0.21
O(1s)	**0.19**	0.52	0.41	0.83	0.23	0.37	0.35	0.41
F(1s)	**0.18**	0.50	0.59	0.99	0.24	0.34	0.43	0.72

[a]Same data set as in Table 2, including atomic relativistic corrections, and with values of β from Table 4. [b]The smallest MAE in each row is presented in boldface and the largest is underlined.

Table 6: Errors in the Lowest Dipole-Allowed Transition Energies Using B3LYP-Based Methods.

Molecule	Transition	Error (eV)[a]						Expt.
		ΔSCF	XTPM	XGTPM	IP-TPM@1/2	IP-TPM@1/3	shifted-XTPM	
Thymine	$O_2(1s \rightarrow \pi^*)$	0.76	1.58	0.45	0.96	0.02	0.77	531.4[b]
	$O_1(1s \rightarrow \pi^*)$	−0.22	1.04	0.22	0.90	−0.16	0.30	532.3[b]
	$N_4(1s \rightarrow \pi^*)$	0.14	1.31	0.57	0.84	−0.09	0.62	401.7[b]
	$N_3(1s \rightarrow \pi^*)$	−0.20	1.02	0.22	0.66	−0.32	0.33	401.5[c]
	$C_8(1s \rightarrow \pi^*)$	1.01	0.89	−0.51	1.33	0.03	0.31	284.9[b]
	$C_7(1s \rightarrow \pi^*)$	−0.42	0.78	−0.10	1.26	0.04	0.24	285.9[b]
	$C_6(1s \rightarrow \pi^*)$	0.03	1.18	0.38	0.09	−1.11	0.67	287.8[b]
	$C_5(1s \rightarrow \pi^*)$	0.16	1.26	0.51	1.55	0.46	0.72	289.4[b]
Mean Error		0.16	1.13	0.22	0.95	−0.14	0.49	
MAE		0.37	1.13	0.37	0.95	0.28	0.49	
Oxazole	$O(1s \rightarrow \pi^*)$	−0.10	1.18	0.37	1.86	−0.04	0.44	535.0[d]
	$O(1s \rightarrow \sigma^*)$	−0.99	−0.14	−0.97	1.39	−1.22	−0.94	538.3[d]
	$O(1s \rightarrow \sigma^*)$	−1.45	−0.76	−1.60	1.01	−1.77	−1.79	539.5[d]
	$N(1s \rightarrow \pi^*)$	−0.21	1.10	0.16	1.86	−0.01	0.48	399.7[d]
	$N(1s \rightarrow \pi^*)$	0.81	1.24	0.32	0.52	−0.13	0.41	401.5[d]
	$C_2(1s \rightarrow \pi^*)$	−0.34	0.79	−0.01	1.80	−0.08	0.29	287.3[d]
	$C_5(1s \rightarrow \pi^*)$	0.07	1.21	0.38	1.64	0.24	0.69	286.5[d]
	$C_4(1s \rightarrow \pi^*)$	0.16	1.36	0.49	1.62	0.34	0.81	286.0[d]
Mean Error		−0.26	0.75	−0.11	1.46	−0.33	0.05	
MAE		0.52	0.97	0.54	1.46	0.48	0.73	

[a]Error defined as theory minus experiment, including atomic relativistic corrections. [b]From Ref. 153. [c]From Ref. 154. [d]From Ref. 155.

calculations, as a convenient and robust alternative to state-by-state approaches such as ΔSCF. Like XGTPM (eq 16), the shifted-XTPM approach requires two different SCF calculations (from which a full spectrum is obtained), yet the latter is somewhat more accurate and also more consistent (or perhaps less erratic) across XC functionals.

D. Other Applications. As illustrative applications, we use several different methods to compute carbon, oxygen, and nitrogen K-edge excitation energies for the thymine and oxazole molecules. Errors (relative to experiment) are listed in Table 6 for a variety of methods, all based on the B3LYP functional. The transitions in question represent the lowest dipole-allowed excitation from each indicated 1s orbital. In the case of thymine, the shifted-XTPM approach affords a MAE of 0.5 eV across the 8 K-edge excitations that are considered, which compares well to ΔSCF results, for which the MAE is 0.4 eV. (The IP-TPM@1/3 method also performs very well but is not charge-neutral and thus not preferred.) Similar trends amongst methods are observed for oxazole, although the MAEs are slightly larger.

Oscillator strengths for the eigenvalue-based methods have been implemented based on eq 2. For methods such as GSTM that involve more than one fractional-electron SCF calculation, Nakajima *et al.*[60] suggest weighting the transition intensities $I_{v\rightarrow c}$ with the same coefficients that are used to combine the eigenvalues. However, we find that the shifted-XTPM approach works somewhat better than GSTM, and requires the same number of SCF cal-

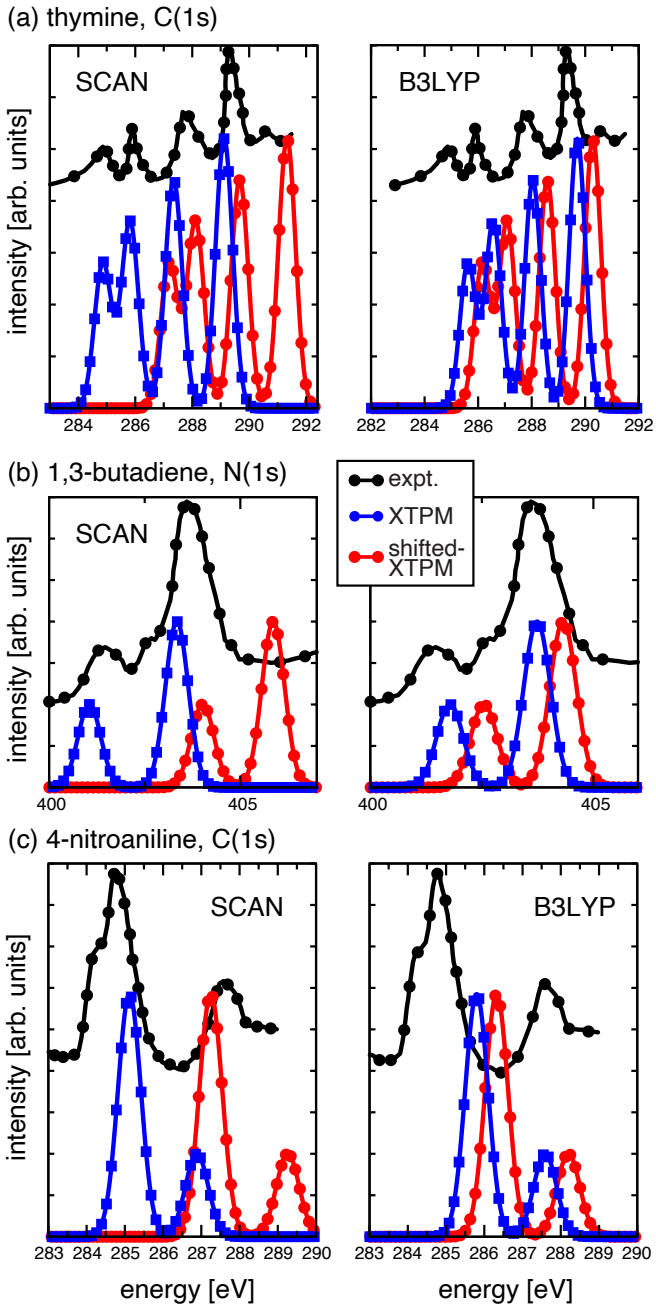

Fig. 2: XAS atomic K-edge spectra for (a) thymine,[153] (b) 1,3-butadiene,[156] and (c) 4-nitroaniline,[157] computing using the SCAN- and B3LYP-based XTPM procedures and their empirically-shifted analogues. Gaussian broadening with $\sigma =$ 0.3 eV is used to obtain spectra from transition energies and oscillator strengths.

culations, therefore we have not computed spectra with GSTM. For the shifted XTPM approach, we use oscillator strengths corresponding to the unshifted method.

Figure 2 shows XAS spectra of thymine (at its carbon K-edge), 1,3-butadiene (carbon K-edge), and 4-nitroaniline (nitrogen K-edge), as compared to experiment, for both the shifted and unshifted XTPM procedure using either SCAN or B3LYP. Empirical shifting corrects the peak positions for either functional, leading to better absolute agreement with experiment, although the peak spacing is scarcely affected. The shifted-XTPM approach may therefore be a useful alternative to TD-DFT for low-lying core-to-valence XAS.

5 Conclusions

The performance of various XC functional approximations has been tested for K-edge excitation energies (1s $\rightarrow$ virtual) involving 1s orbitals of second-row elements. These methods include both ΔSCF and also fractional-electron approaches that originate in Slater's transition approximation, which use Kohn-Sham eigenvalues (only), from one or more modified SCF calculations, in order to obtain an excitation spectrum. The overall conclusions are as follows.

- For ΔSCF calculations, the SCAN, SCAN0 and B3LYP functionals are recommended. Each exhibits a statistical accuracy (for the absolute excitation energy) of 0.3 eV when an atomic relativistic correction is used. In contrast, the LRC-ωPBE functional that is widely used in TD-DFT calculations, and the SRC1-r1 functional that was specifically parameterized for for K-edge TD-DFT, exhibit MAEs greater than 1 eV and are not recommended for ΔSCF calculations.

- For the same benchmarks, a generalized version of Slater's method (GSTM) is also useful, if the functional is carefully selected. In conjunction with either B3LYP or LRC-ωPBEh, GSTM affords an absolute accuracy of 0.3–0.4 eV. This method requires two fractional-occupancy SCF calculations per elemental edge but not state-by-state calculation of the higher-lying excitations, and should therefore be more robust against variational collapse as compared to ΔSCF calculations.

- Other methods including TPM, GTPM, FCHM, and XCHM afford larger errors and cannot be recommended, despite their continued widespread use. For example, the best we are able to do with XCHM is an overall error of about 1.6 eV when used with the SCAN functional; this is much larger than the ΔSCF error (0.3 eV) obtained using the same functional. For TPM, the smallest overall error is 2.9 eV (using B3LYP), for GTPM it is 2.2 eV (again using B3LYP), and for FCHM it is 1.8 eV (in conjunction with BH&HLYP). Each of these errors is significantly larger than the ΔSCF error for the same functional.

- The IP-TPM@1/3 protocol introduced here affords errors of about 0.3 eV when used with B3LYP,

which is comparable to the ΔSCF accuracy. However, this method requires the creation of a charged excitation, which is not well suited for periodic calculations.

- For higher-lying excitations (involving virtual orbitals beyond the LUMO), errors are larger for the eigenvalue-based methods although XTPM-B3LYP and XGTPM-B3LYP afford absolute accuracies of 0.7 and 0.8 eV, respectively. B3LYP-based ΔSCF calculations afford an accuracy of 0.3 eV for the same data set.

- To improve XTPM, which is based on a single fractional-occupancy SCF calculations, we introduce a simple shifting procedure. When used with SCAN or B3LYP, this approach achieves an accuracy of 0.3 eV (SCAN) or 0.5 eV (B3LYP), for 1s → LUMO transitions. For higher-lying excitations, the MAE is 0.6 eV for both functionals and this is as good as far more expensive many-body techniques such as BSE@G_0W_0. When combined with oscillator strengths based on transition dipole moments between MOs, reasonable XAS spectra are obtained for several molecules.

Overall, the shifted-XTPM approach is competitive with the best *ab initio* techniques for K-edge core-to-valence transition energies, just as the shifted-STM procedure is one of the most accurate methods for K-shell CEBEs.[44] This method is based on an easy-to-converge fractional-electron procedure that does not require promotion of any electrons beyond the LUMO, making it relatively robust against variational collapse. The shifted-STM approach should be a useful tool for simulating core-level XAS and XPS in complicated environments and large molecular systems.

Supporting Information

Complete results for each of the data set, methods, and XC functionals considered here.

Acknowledgments

This work was supported by the U.S. Department of Energy, Office of Basic Energy Sciences, Division of Chemical Sciences, Geosciences, and Biosciences (Award No. DE-SC0008550), and by the National Science Foundation (Grant No. CHE-1955282). Calculations were performed at the Ohio Supercomputer Center.[158]

Author Declarations

J.M.H. serves on the board of directors of Q-Chem Inc.

[1] Penner-Hahn, J. E. X-ray absorption spectroscopy in coordination chemistry. *Coord. Chem. Rev.* **1999,** *190–192,* 1101–1123.

[2] de Groot, F.; Kotani, A. *Core Level Spectroscopy of Solids;* CRC Press: Boca Raton, 2008.

[3] Kleine, C.; Ekimova, M.; Goldsztejn, G.; Raabe, S.; Strüber, C.; Ludwig, J.; Yarlagadda, S.; Eisebitt, S.; Vrakking, M. J. J.; Elsaesser, T.; Nibbering, E. T. J.; Rouzée, A. Soft x-ray absorption spectroscopy of aqueous solutions using a table-top femtosecond soft x-ray source. *J. Phys. Chem. Lett.* **2019,** *10,* 52–58.

[4] Aarva, A.; Deringer, V. L.; Sainio, S.; Laurila, T.; Caro, M. A. Understanding x-ray spectroscopy of carbonaceous materials by combining experiments, density functional theory, and machine learning. Part I: Fingerprint spectra. *Chem. Mater.* **2019,** *31,* 9243–9255.

[5] Aarva, A.; Deringer, V. L.; Sainio, S.; Laurila, T.; Caro, M. A. Understanding x-ray spectroscopy of carbonaceous materials by combining experiments, density functional theory, and machine learning. Part II: Quantitative fitting of spectra. *Chem. Mater.* **2019,** *31,* 9256–9267.

[6] Deng, Y.; Gao, B.; Deng, M.; Luo, Y. A comparative theoretical study on core-hole excitation spectra of azafullerene and its derivatives. *J. Chem. Phys.* **2014,** *140,* 124304:1–11.

[7] Stetina, T. F.; Clark, A. E.; Li, X. X-ray absorption signatures of hydrogen-bond structure in water–alcohol solutions. *Int. J. Quantum Chem.* **2018,** *119,* e25802:1–6.

[8] Bari, S. *et al.* Soft x-ray spectroscopy as a probe for gas-phase protein structure: Electron impact ionization from within. *Chem. Eur. J.* **2018,** *24,* 7631–7636.

[9] Paszkiewicz, M.; Biktagirov, T.; Aldahhak, H.; Allegretti, F.; Rauls, E.; Schöfberger, W.; Schmidt, W. G.; Barth, J. V.; Gerstmann, U.; Klappenberger, F. Unraveling the oxidation and spin state of Mn–corrole through x-ray spectroscopy and quantum chemical analysis. *J. Phys. Chem. Lett.* **2018,** *9,* 6412–6420.

[10] Persson, I.; Trublet, M.; Klysubun, W. Structure determination of phosphoric acid and phosphate ions in aqueous solution using EXAFS spectroscopy and large angle x-ray scattering. *J. Phys. Chem. A* **2018,** *122,* 7413–7420.

[11] Sergentu, D.-C.; Duignan, T. J.; Autschbach, J. Ab initio study of covalency in the ground versus core-excited states and x-ray absorption spectra of actinide complexes. *J. Phys. Chem. Lett.* **2018,** *9,* 5582–5591.

[12] Zhovtobriukh, I.; Norman, P.; Pettersson, L. G. M. X-ray absorption spectrum simulations of hexagonal ice. *J. Chem. Phys.* **2019,** *150,* 034501:1–14.

[13] Norman, P.; Dreuw, A. Simulating x-ray spectroscopies and calculating core-excited states of molecules. *Chem. Rev.* **2018,** *118,* 7208–7248.

[14] Bokarev, S. I.; Kühn, O. Theoretical x-ray spectroscopy of transition metal compounds. *WIREs Comput. Mol. Sci.* **2020,** *10,* e1433:1–36.

[15] Kasper, J. M.; Stetina, T. F.; Jenkins, A. J.; Li, X. *Ab initio* methods for L-edge x-ray absorption spectroscopy. *Chem. Phys. Rev.* **2020,** *1,* 011304.

[16] Rankine, C. D.; Penfold, T. J. Progress in the theory of x-ray spectroscopy: From quantum chemistry to machine learning and ultrafast dynamics. *J. Phys. Chem. A* **2021,** *125,* 4276–4293.

[17] Tsuru, S.; Vidal, M. L.; Pápaii, M.; Krylov, A. I.; Møller, K. B.; Coriani, S. An assessment of different electronic structure approaches for modeling time-resolved x-ray absorption spectroscopy. *Struct. Dynam.* **2021,** *8,* 024101:1–15.

[18] Klein, B. P.; Hall, S. J.; Mauer, R. J. The nuts and bolts of core-hole constrained *ab initio* simulation for K-shell x-ray photoemission and absorption spectra. *J. Phys.: Condens. Matt.* **2021,** *33,* 154005:1–20.

[19] Besley, N. A. Density functional theory based methods for the calculation of x-ray spectroscopy. *Acc. Chem. Res.* **2020,** *53,* 1306–1315.

[20] Besley, N. A. Modeling of the spectroscopy of core electrons with density functional theory. *WIREs Comput. Mol. Sci.* **2021,** *12,* e1527:1–22.

[21] Herbert, J. M. Density-functional theory for electronic excited states. In *Theoretical and Computational Photochemistry: Fundamentals, Methods, Applications and Synergy with Experimental Approaches*; García-Iriepa, C.; Marazzi, M., Eds.; Elsevier: 2023; Chapter 3, pages 69–118.

[22] Nascimento, D. R.; Govind, N. Computational approaches for XANES, VtC-XES, and RIXS using linear-response time-dependent density functional theory based methods. *Phys. Chem. Chem. Phys.* **2022,** *24,* 14680–14691.

[23] Annegarn, M.; Kahk, J. M.; Lischner, J. Combining time-dependent density functional theory and the ΔSCF approach for accurate core-electron spectra. *J. Chem. Theory Comput.* **2022,** *18,* 7620–7629.

[24] Carter-Fenk, K.; Cunha, L. A.; Arias-Martinez, J. E.; Head-Gordon, M. Electron-affinity time-dependent density functional theory: Formalism and applications to core-excited states. *J. Phys. Chem. Lett.* **2022,** *13,* 9664–9672.

[25] Hanson-Heine, M. W. D.; George, M. W.; Besley, N. A. Calculating excited state properties using Kohn-Sham density functional theory. *J. Chem. Phys.* **2013,** *138,* 064101:1–8.

[26] Hait, D.; Haugen, E. A.; Yang, Z.; Oosterbaan, K. J.; Leone, S. R.; Head-Gordon, M. Accurate prediction of core-level spectra of radicals at density functional theory cost via square gradient minimization and recoupling of mixed configurations. *J. Chem. Phys.* **2020,** *153,* 134108:1–14.

[27] Hait, D.; Head-Gordon, M. Highly accurate prediction of core spectra of molecules at density functional theory cost: Attaining sub-electronvolt error from a restricted open-shell Kohn–Sham approach. *J. Phys. Chem. Lett.* **2020,** *11,* 775–786.

[28] Cunha, L. A.; Hait, D.; Kang, R.; Mao, Y.; Head-Gordon, M. Relativistic orbital-optimized density functional theory for accurate core-level spectroscopy. *J. Phys. Chem. Lett.* **2022,** *13,* 3438–3449.

[29] Rehn, D. R.; Dreuw, A.; Norman, P. Resonant inelastic x-ray scattering amplitudes and cross sections in the algebraic diagrammatic construction/intermediate state representation (ADC/ISR) approach. *J. Chem. Theory Comput.* **2017,** *13,* 5552–5559.

[30] Fransson, T.; Dreuw, A. Simulating x-ray emission spectroscopy with algebraic diagrammatic construction schemes for the polarization propagator. *J. Chem. Theory Comput.* **2019,** *15,* 546–556.

[31] Vidal, M. L.; Feng, X.; Epifanovsky, E.; Krylov, A. I.; Coriani, S. New and efficient equation-of-motion coupled-cluster framework for core-excited and core-ionized states. *J. Chem. Theory Comput.* **2019,** *15,* 3117–3133.

[32] Vidal, M. L.; Pokhilko, P.; Krylov, A. I.; Coriani, S. Equation-of-motion coupled-cluster theory to model L-edge x-ray absorption and photoelectron spectroscopy. *J. Phys. Chem. Lett.* **2020,** *11,* 8314–8321.

[33] Vinson, J.; Rehr, J. J.; Kas, J. J.; Shirley, E. L. Bethe-Salpeter equation calculations of core excitation spectra. *Phys. Rev. B* **2011,** *83,* 115106:1–7.

[34] Vinson, J.; Rehr, J. J. *Ab initio* Bethe-Salpeter calculations of the x-ray absorption spectra of transition metals at the L-shell edges. *Phys. Rev. B* **2012,** *86,* 195135:1–6.

[35] Aoki, T.; Ohno, K. *Ab initio* simulations of x-ray emission spectroscopy with the GW + Bethe-Salpeter equation method. *Phys. Rev. B* **2019,** *100,* 075149:1–9.

[36] Yao, Y.; Golze, D.; Rinke, P.; Blum, V.; Kanai, Y. All-electron BSE@GW method for K-edge core electron excitation energies. *J. Chem. Theory Comput.* **2022,** *18,* 1569–1583.

[37] Unzog, M.; Tal, A.; Kresse, G. X-ray absorption using the projector augmented-wave method and the Bethe-Salpeter equation. *Phys. Rev. B* **2022,** *106,* 155133:1–16.

[38] Nakata, A.; Imamura, Y.; Otsuka, T.; Nakai, H. Time-dependent density functional theory calculations for core-excited states: Assessment of standard exchange-correlation functionals and development of a novel hybrid functional. *J. Chem. Phys.* **2006,** *124,* 094105:1–9.

[39] Nakata, A.; Imamura, Y.; Nakai, H. Hybrid exchange-correlation functional for core, valence, and Rydberg excitations: Core-valence-Rydberg B3LYP. *J. Chem. Phys.* **2006,** *125,* 064109:1–9.

[40] Besley, N. A.; Peach, M. J. G.; Tozer, D. J. Time-dependent density functional theory calculations of near-edge x-ray absorption fine structure with short-range corrected functionals. *Phys. Chem. Chem. Phys.* **2009,** *11,* 10350–10358.

[41] Besley, N. A.; Asmuruf, F. A. Time-dependent density functional theory calculations of the spectroscopy of core electrons. *Phys. Chem. Chem. Phys.* **2010,** *12,* 12024–12039.

[42] Nakata, A.; Imamura, Y.; Nakai, H. Extension of the core-valence-Rydberg B3LYP functional to core-excited-state calculations of third-row atoms. *J. Chem. Theory Comput.* **2007,** *3,* 1295–1305.

[43] Roemelt, M.; Beckwith, M. A.; Duboc, C.; Collomb, M.-N.; Neese, F.; DeBeer, S. Manganese K-edge x-ray absorption spectroscopy as a probe of metal–ligand interactions in coordination compounds. *Inorg. Chem.* **2012,** *51,* 680–687.

[44] Jana, S.; Herbert, J. M. Slater transition methods for core-level electron binding energies. *J. Chem. Phys.* **2023,** *158,* 094111:1–14.

[45] Geneaux, R.; Marroux, H. J. B.; Guggenmos, A.; Neu-

mark, D. M.; Leone, S. R. Transient absorption spectroscopy using high harmonic generation: A review of ultrafast x-ray dynamics in molecules and solids. *Phil. Trans. R. Soc. A* **2019,** *377,* 20170463:1–27.

[46] Liu, H.; Klein, I. M.; Michelsen, J. M.; Cushing, S. K. Element-specific electronic and structural dynamics using transient XUV and soft x-ray spectroscopy. *Chem* **2021,** *7,* 2569–2584.

[47] Cavaletto, S. M.; Nascimento, D. R.; Zhang, Y.; Govind, N.; Mukamel, S. Resonant stimulated x-ray Raman spectroscopy of mixed-valence manganese complexes. *J. Phys. Chem. Lett.* **2021,** *12,* 5925–5931.

[48] Loe, C. M.; Liekhus-Schmaltz, C.; Govind, N.; Khalil, M. Spectral signatures of ultrafast excited-state intramolecular proton transfer from computational multi-edge transient x-ray absorption spectroscopy. *J. Phys. Chem. Lett.* **2021,** *12,* 9840–9847.

[49] Biswas, S.; Baker, L. R. Extreme ultraviolet reflection–absorption spectroscopy: Probing dynamics at surfaces from a molecular perspective. *Acc. Chem. Res.* **2022,** *55,* 893–903.

[50] Mayer, D. *et al.* Following excited-state chemical shifts in molecular ultrafast x-ray photoelectron spectroscopy. *Nat. Commun.* **2022,** *13,* 198:1–9.

[51] Michelitsch, G. S.; Reuter, K. Efficient simulation of near-edge x-ray absorption fine structure (NEXAFS) in density-functional theory: Comparison of core-level constraining approaches. *J. Chem. Phys.* **2019,** *150,* 074104:1–12.

[52] Slater, J. C.; Wood, J. H. Statistical exchange and the total energy of a crystal. *Int. J. Quantum Chem.* **1971,** *5,* 3–34.

[53] Slater, J. C. Statistical exchange-correlation in the self-consistent field. *Adv. Quantum Chem.* **1972,** *6,* 1–92.

[54] Slater, J. C.; Johnson, K. H. Self-consistent-field $X\alpha$ cluster method for polyatomic molecules and solids. *Phys. Rev. B* **1972,** *5,* 844–853.

[55] Stener, M.; Lisini, A.; Decleva, P. Density functional calculations of excitation energies and oscillator strengths for C1s $\rightarrow \pi^*$ and O1s $\rightarrow \pi^*$ excitations and ionization potentials in carbonyl containing molecules. *Chem. Phys.* **1995,** *191,* 141–154.

[56] Stöhr, J. *NEXAFS Spectroscopy;* volume 25 of *Springer Series in Surface Sciences* Springer-Verlag: Berlin, 1st ed.; 1996.

[57] Schwarz, K. On Slater's transition state for ionization energies. *Chem. Phys.* **1975,** *7,* 100–107.

[58] Williams, A. R.; deGroot, R. A.; Sommers, C. B. Generalization of Slater's transition state concept. *J. Chem. Phys.* **1975,** *63,* 628–631.

[59] Hirao, K.; Nakajima, T.; Chan, B. An improved Slater's transition state approximation. *J. Chem. Phys.* **2021,** *155,* 034101:1–9.

[60] Nakajima, T.; Hirao, K.; Chan, B. Higher-order transition state approximation. *J. Chem. Phys.* **2022,** *156,* 114112:1–7.

[61] Triguero, L.; Pettersson, L. G. M.; Ågren, H. Calculations of near-edge x-ray-absorption spectra of gas-phase and chemisorbed molecules by means of density-functional and transition-potential theory. *Phys. Rev. B* **1998,** *58,* 8097–8110.

[62] Triguero, L.; Pettersson, L. G. M.; Ågren, H. Calculations of x-ray emission spectra of molecules and surface adsorbates by means of density functional theory. *J. Phys. Chem. A* **1998,** *102,* 10599–10607.

[63] Triguero, L.; Plashkevych, O.; Pettersson, L. G. M.; Ågren, H. Separate state vs. transition state Kohn-Sham calculations of x-ray photoelectron binding energies and chemical shifts. *J. Electron Spectrosc.* **1999,** *104,* 195–207.

[64] Prendergast, D.; Galli, G. X-ray absorption spectra of water from first principles calculations. *Phys. Rev. Lett.* **2006,** *96,* 215502:1–4.

[65] Tanaka, I.; Araki, H.; Yoshiya, M.; Mizoguchi, T.; Ogasawara, K.; Adachi, H. First-principles calculations of electron-energy-loss near-edge structure and near-edgge x-ray-absorption fine structure of BN polytypes using model clusters. *Phys. Rev. B* **1999,** *60,* 4944–4951.

[66] Hetényi, B.; De Angelis, F.; Giannozzi, P.; Car, R. Calculation of near-edge x-ray-absorption fine structure at finite temperatures: Spectral signatures of hydrogen bond breaking in liquid water. *J. Chem. Phys.* **2004,** *120,* 8632–8637 Erratum: *ibid.* **124**, 099901 (2006).

[67] Leetmaa, M.; Ljungberg, M. P.; Lyubartsev, A.; Nilsson, A.; Pettersson, L. G. M. Theoretical approximations to x-ray absorption spectroscopy of liquid water and ice. *J. Electron Spectrosc.* **2010,** *177,* 135–157.

[68] Kolczewski, C.; Püttner, R.; Plashkevych, O.; Ågren, H.; Staemmler, V.; Martins, M.; Snell, G.; Schlachter, A. S.; Sant'Anna, M.; Kaindl, G.; Pettersson, L. G. M. Detailed study of pyridine at the C1s and N1s ionization thresholds: The influence of the vibrational fine structure. *J. Chem. Phys.* **2001,** *115,* 6426–6437.

[69] Gilbert, A. T. B.; Besley, N. A.; Gill, P. M. W. Self-consistent field calculations of excited states using the maximum overlap method (MOM). *J. Phys. Chem. A* **2008,** *112,* 13164–13171.

[70] Barca, G. M. J.; Gilbert, A. T. B.; Gill, P. M. W. Simple models for difficult electronic excitations. *J. Chem. Theory Comput.* **2018,** *14,* 1501–1509.

[71] Corzo, H. H.; Taka, A. A.; Pribam-Jones, A.; Hratchian, H. P. Using projection operators with maximum overlap methods to simplify challenging self-consistent field optimization. *J. Comput. Chem.* **2022,** *43,* 382–390.

[72] Hait, D.; Head-Gordon, M. Excited state orbital optimization via minimizing the square of the gradient: General approach and application to singly and doubly excited states via density functional theory. *J. Chem. Theory Comput.* **2020,** *16,* 1699–1710.

[73] Carter-Fenk, K.; Herbert, J. M. State-targeted energy projection: A simple and robust approach to orbital relaxation of non-Aufbau self-consistent field solutions. *J. Chem. Theory Comput.* **2020,** *16,* 5067–5082.

[74] Besley, N. A.; Gilbert, A. T. B.; Gill, P. M. W. Self-consistent-field calculations of core excited states. *J. Chem. Phys.* **2009,** *130,* 124308:1–7.

[75] Vydrov, O. A.; Scuseria, G. E.; Perdew, J. P. Tests of functionals for systems with fractional electron number. *J. Chem. Phys.* **2007,** *126,* 154109:1–9.

[76] Cohen, A. J.; Mori-Sanchez, P.; Yang, W. Insights into current limitations of density functional theory. *Science* **2008,** *321,* 792–794.

[77] Ferreira, L. G.; Marques, M.; Teles, L. K. Approximation to density functional theory for the calculation of band gaps of semiconductors. *Phys. Rev. B* **2008,** *78,* 125116:1–9.

[78] Ferreira, L. G.; Marques, M.; Teles, L. K. Slater half-occupation technique revisited: The LDA-1/2 and GGA-

1/2 approaches for atomic ionization energies and band gaps in semiconductors. *AIP Adv.* **2011,** *1,* 032119:1–11.

[79] Tsudeda, T.; Song, J.-W.; Suzuki, S.; Hirao, K. On Koopmans' theorem in density functional theory. *J. Chem. Phys.* **2010,** *133,* 174101:1–9.

[80] Autschbach, J.; Srebro, M. Delocalization error and "functional tuning" in Kohn-Sham calculations of molecular properties. *Acc. Chem. Res.* **2014,** *47,* 2592–2602.

[81] Sadigh, B.; Erhart, P.; Åberg, D. Variational polaron self-interaction-corrected total-energy functional for charge excitations in insulators. *Phys. Rev. B* **2015,** *92,* 075202:1–10 Erratum: *ibid.* **92**, 199905(E) (2015).

[82] Bajaj, A.; Janet, J. P.; Kulik, H. J. Communication: Recovering the flat-plane condition in electronic structure theory at semi-local DFT cost. *J. Chem. Phys.* **2017,** *147,* 191101:1–5.

[83] Hirao, K.; Nakajima, T.; Chan, B.; Lee, H.-J. The core ionization energies calculated by delta SCF and Slater's transition state theory. *J. Chem. Phys.* **2023,** *158,* 064112:1–17.

[84] Steinmann, S. N.; Yang, W. Wave function methods for fractional electrons. *J. Chem. Phys.* **2013,** *139,* 074107:1–14.

[85] Ehlert, C.; Klamroth, T. The quest for best suited references for configuration interaction singles calculations of core excited states. *J. Comput. Chem.* **2017,** *38,* 116–126.

[86] Simons, M.; Matthews, D. A. Transition-potential coupled cluster. *J. Chem. Phys.* **2021,** *154,* 014106:1–9.

[87] Simons, M.; Matthews, D. A. Transition-potential coupled cluster II: Optimisation of the core orbital occupation number. *Mol. Phys.* **2023,** e2088421:1–9.

[88] Janak, J. F. Proof that $\partial E/\partial n_i = \epsilon_i$ in density-functional theory. *Phys. Rev. B* **1978,** *18,* 7165–7168.

[89] Chong, D. P. Accurate calculation of core–electron binding energies by the density-functional method. *Chem. Phys. Lett.* **1995,** *232,* 486–490.

[90] Chong, D. P. Density-functional calculation of core-electron binding energies of C, N, O, and F. *J. Chem. Phys.* **1995,** *103,* 1842–1845.

[91] Hu, C.-H.; Chong, D. P. Density functional computations for inner-shell excitation spectroscopy. *Chem. Phys. Lett.* **1996,** *262,* 729–732.

[92] Cavigliasso, G.; Chong, D. P. Accurate density-functional calculation of core-electron binding energies by a total-energy difference approach. *J. Chem. Phys.* **1999,** *111,* 9485–9492.

[93] Zhang, Y.; Hua, W.; Bennett, K.; Mukamel, S. Nonlinear spectroscopy of core and valence excitations using short x-ray pulses: Simulation challenges. In *Density-Functional Methods for Excited States*, Vol. 368; Ferré, N.; Filatov, M.; Huix-Rotllant, M., Eds.; Springer International Publishing: Cham, Switzerland, 2016.

[94] Taucher, T. C.; Hofmann, O. T.; Zojer, E. Final-state simulations of core-level binding energies at metal-organic hybrid interfaces: Artifacts caused by spurious collective electrostatic effects. *ACS Omega* **2020,** *5,* 25868–25881.

[95] Kimber, P.; Plasser, F. Toward an understanding of electronic excitation energies beyond the molecular orbital picture. *Phys. Chem. Chem. Phys.* **2020,** *22,* 6058–6080.

[96] Kimber, P.; Plasser, F. Energy component analysis for electronically excited states of molecules: Why the lowest excited state is not always the HOMO/LUMO transition. *J. Chem. Theory Comput.* **2023,** *19,* 2340–2352.

[97] Pickup, B. T.; Goscinski, O. Direct calculation of ionization energies. I. Closed shells. *Mol. Phys.* **1973,** *26,* 1013–1035.

[98] Goscinski, O.; Pickup, B. T.; Purvis, G. Direct calculation of ionization energies. Transition operator for the ΔE_{SCF} method. *Chem. Phys. Lett.* **1973,** *22,* 167–171.

[99] Pickup, B. T. Extended Koopmans' theorem and sudden ionization processes. *Chem. Phys. Lett.* **1975,** *33,* 422–426.

[100] Opoku, E.; Pawłowski, F.; Ortiz, J. V. A new generation of diagonal self-energies for the calculation of electron removal energies. *J. Chem. Phys.* **2021,** *155,* 204107:1–17.

[101] Zamani, A. Y.; Hratchian, H. P. Assessing the performance of ΔSCF and the diagonal second-order self-energy approximation for calculating vertical core excitation energies. *J. Chem. Phys.* **2022,** *157,* 084115:1–10.

[102] Kimber, P.; Plasser, F. Classification and analysis of molecular excited states. In *Comprehensive Computational Chemistry*; Elsevier: 2023.

[103] Cederbaum, L. S.; Domcke, W.; Schirmer, J.; von Niessen, W. Correlation effects in the ionization of molecules: Breakdown of the molecular orbital picture. *Adv. Chem. Phys.* **1986,** *65,* 115–159.

[104] Liang, Y.; Vinson, J.; Pemmaraju, S.; Drisdell, W. S.; Shirley, E. L.; Prendergast, D. Accurate x-ray spectral predictions: An advanced self-consistent-field approach inspired by many-body perturbation theory. *Phys. Rev. Lett.* **2017,** *118,* 096402:1–7.

[105] Epifanovsky, E. *et al.* Software for the frontiers of quantum chemistry: An overview of developments in the Q-Chem 5 package. *J. Chem. Phys.* **2021,** *155,* 084801:1–59.

[106] Sun, J.; Ruzsinszky, A.; Perdew, J. P. Strongly constrained and appropriately normed semilocal density functional. *Phys. Rev. Lett.* **2015,** *115,* 036402:1–6.

[107] Hui, K.; Chai, J.-D. SCAN-based hybrid and double-hybrid density functionals from models without fitted parameters. *J. Chem. Phys.* **2016,** *144,* 044114:1–7.

[108] Becke, A. D. Density-functional thermochemistry. III. The role of exact exchange. *J. Chem. Phys.* **1993,** *98,* 5648–5652.

[109] Lee, C.; Yang, W.; Parr, R. G. Development of the Colle-Salvetti correlation-energy formula into a functional of the electron density. *Phys. Rev. B* **1988,** *37,* 785–789.

[110] Mardirossian, N.; Head-Gordon, M. ωB97X-V: A 10-parameter, range-separated hybrid, generalized gradient approximation density functional with nonlocal correlation, designed by a survival-of-the-fittest strategy. *Phys. Chem. Chem. Phys.* **2014,** *16,* 9904–9924.

[111] Yanai, T.; Tew, D. P.; Handy, N. C. A new hybrid exchange-correlation functional using the Coulomb-attenuating method (CAM-B3LYP). *Chem. Phys. Lett.* **2004,** *393,* 51–57.

[112] Rohrdanz, M. A.; Herbert, J. M. Simultaneous benchmarking of ground- and excited-state properties with long-range-corrected density functional theory. *J. Chem. Phys.* **2008,** *129,* 034107:1–9.

[113] Rohrdanz, M. A.; Martins, K. M.; Herbert, J. M. A long-range-corrected density functional that performs well for both ground-state properties and time-dependent density functional theory excitation energies, including charge-transfer excited states. *J. Chem. Phys.* **2009,** *130,* 054112:1–8.

[114] Lange, A. W.; Herbert, J. M. Both intra- and interstrand charge-transfer excited states in B-DNA are present at energies comparable to, or just above, the $^1\pi\pi^*$ excitonic

bright states. *J. Am. Chem. Soc.* **2009,** *131,* 3913–3922.
[115] Zhu, Y.; Alam, B.; Herbert, J. M. Broadband x-ray absorption spectra from time-dependent Kohn-Sham calculations. **2021,** .
[116] Gill, P. M. W.; Johnson, B. G.; Pople, J. A. A standard grid for density-functional calculations. *Chem. Phys. Lett.* **1993,** *209,* 506–512.
[117] Dasgupta, S.; Herbert, J. M. Standard grids for high-precision integration of modern density functionals: SG-2 and SG-3. *J. Comput. Chem.* **2017,** *38,* 869–882.
[118] Furness, J. W.; Kaplan, A. D.; Ning, J.; Perdew, J. P.; Sun, J. Accurate and numerically efficient r^2SCAN meta-generalized gradient approximation. *J. Phys. Chem. Lett.* **2020,** *11,* 8208–8215 Erratum: *ibid.* **11**, 9248 (2020).
[119] Subotnik, J. E.; Shao, Y.; Liang, W.; Head-Gordon, M. An efficient method for calculating maxima of homogeneous functions of orthogonal matrices: Applications to localized occupied orbitals. *J. Chem. Phys.* **2004,** *121,* 9220–9229.
[120] Schwarz, W. H. E.; Chang, T. C. Multiconfiguration wave functions for highly excited states by the generalized Brillouin theorem method. *Int. J. Quantum Chem. Symp.* **1976,** *10,* 91–97.
[121] Cederbaum, L. S.; Domcke, W. Localized and delocalized core holes and their interrelation. *J. Chem. Phys.* **1977,** *66,* 5084–5086.
[122] Schwarz, W. H. E.; Chang, T. C.; Seeger, U.; Hwang, K. H. Core excitations of symmetrical aromatic molecules. Specific correlations in the valence shell and localization in the core shells. *Chem. Phys.* **1987,** *117,* 73–89.
[123] Brumboiu, I. E.; Fransson, T. Core–hole delocalization for modeling x-ray spectroscopies: A cautionary tale. *J. Chem. Phys.* **2022,** *156,* 214109:1–13.
[124] Snyder, L. C. Core-electron binding energies and Slater atomic shielding constants. *J. Chem. Phys.* **1971,** *55,* 95–99.
[125] Broer, R.; Nieuwpoort, W. C. Broken orbital-symmetry and the description of hole states in the tetrahedral $[CrO_4]^-$ anion. I. Introductory considerations and calculations on oxygen 1s hole states. *Chem. Phys.* **1981,** *54,* 291–303.
[126] Ma, Y.; Sette, F.; Meigs, G.; Modesti, S.; Chen, C. T. Breaking of ground-state symmetry in core-excited ethylene and benzene. *Phys. Rev. Lett.* **1989,** *63,* 2044–2047.
[127] Takahashi, O. Relativistic corrections for single- and double-core excitations at the K- and L-edges from Li to Kr. *Comput. Theor. Chem.* **2017,** *1102,* 80–86.
[128] Hait, D.; Oosterbaan, K. J.; Carter-Fenk, K.; Head-Gordon, M. Computing x-ray absorption spectra from linear-response particles atop optimized holes. *J. Chem. Phys.* **2022,** *156,* 201104:1–9.
[129] Takahashi, O.; Pettersson, L. G. M. Functional dependence of core-excitation energies. *J. Chem. Phys.* **2004,** *121,* 10339–10345.
[130] El-Nahas, A. M.; Simmie, J. M.; Mangood, A. H.; Hirao, K.; Song, J.-W.; Watson, M. A.; Taketsugu, T.; Koga, N. Assessment of hybrid, meta-hybrid-GGA, and long-range corrected density functionals for the estimation of enthalpies of formation, barrier heights, and ionisation potentials of selected C1–C5 oxygenates. *Mol. Phys.* **2015,** *113,* 1630–1635.
[131] Hirao, K.; Bae, H.-S.; Song, J.-W.; Chan, B. Koopmans'-type theorem in Kohn–Sham theory with optimally tuned long-range-corrected (LC) functionals. *J. Phys. Chem. A* **2021,** *125,* 3489–3502.
[132] Song, J.-W.; Watson, M. A.; Nakata, A.; Hirao, K. Core-excitation energy calculations with a long-range corrected hybrid exchange-correlation functional including a short-range Gaussian attenuation (LCgau-BOP). *J. Chem. Phys.* **2008,** *129,* 184113:1–9.
[133] Baer, R.; Livshits, E.; Salzner, U. Tuned range-separated hybrids in density functional theory. *Annu. Rev. Phys. Chem.* **2010,** *61,* 85–109.
[134] Körzdörfer, T.; Sears, J. S.; Sutton, C.; Brédas, J.-L. Long-range corrected hybrid functionals for π-conjugated systems: Dependence of the range-separation parameter on conjugation length. *J. Chem. Phys.* **2011,** *135,* 204107:1–6.
[135] Uhlig, F.; Herbert, J. M.; Coons, M. P.; Jungwirth, P. Optical spectroscopy of the bulk and interfacial hydrated electron from ab initio calculations. *J. Phys. Chem. A* **2014,** *118,* 7507–7515.
[136] Bois, J.; Körzdörfer, T. Size-dependence of nonempirically tuned DFT starting points for G_0W_0 applied to π-conjugated molecular chains. *J. Chem. Theory Comput.* **2017,** *13,* 4962–4971.
[137] Alam, B.; Morrison, A. F.; Herbert, J. M. Charge separation and charge transfer in the low-lying excited states of pentacene. *J. Phys. Chem. C* **2020,** *124,* 24653–24666.
[138] Fransson, T.; Zhotobriukh, I.; Coriani, S.; Wikfeldt, K. T.; Norman, P.; Pettersson, L. G. M. Requirements of first-principles calculations of x-ray absorption spectra of liquid water. *Phys. Chem. Chem. Phys.* **2016,** *18,* 566–583.
[139] Perera, S. D.; Urquhart, S. G. Systematic investigation of π–π interactions in near-edge x-ray fine structure (NEXAFS) spectroscopy of paracyclophanes. *J. Phys. Chem. A* **2017,** *121,* 4907–4913.
[140] Shokatian, S.; Urquhart, S. Near edge X-ray absorption fine structure spectra of linear *n*-alkanes: Variation with chain length. *J. Electron Spectrosc.* **2019,** *236,* 18–26.
[141] Rodrigues, G. L. S.; Diesen, E.; Voss, J.; Norman, P.; Pettersson, L. G. M. Simulations of x-ray absorption spectra for CO desorbing from Ru(0001) with transition-potential and time-dependent density functional theory approaches. *Struct. Dynam.* **2022,** *9,* 014101:1–11.
[142] de Clermont Gallerande, E.; Cabaret, D.; Lelong, G.; Brouder, C.; Attaiaa, M.-B.; Paulatto, L.; Gilmore, K.; Sahle, C. J.; Radtke, G. First-principles modeling of x-ray Raman scattering spectra. *Phys. Rev. B* **2018,** *98,* 214104:1–14.
[143] Kulik, H. J.; Marzari, N.; Correa, A. A.; Prendergast, D.; Schwegler, E.; Galli, G. Local effects in the x-ray absorption spectrum of salt water. *J. Phys. Chem. B* **2010,** *114,* 9594–9601.
[144] Kulik, H. J.; Schwegler, E.; Galli, G. Probing the structure of salt water under confinement with first-principles molecular dynamics and theoretical x-ray absorption spectroscopy. *J. Phys. Chem. Lett.* **2012,** *3,* 2653–2658.
[145] Jiang, P.; Prendergast, D.; Borondics, F.; Porsgaard, S.; Giovanetti, L.; Pach, E.; Newberg, J.; Bluhm, H.; Besenbacher, F.; Salmeron, M. Experimental and theoretical investigation of the electronic structure of Cu_2O and CuO thin films on Cu(110) using x-ray photoelectron and absorption spectroscopy. *J. Chem. Phys.* **2013,** *138,* 024704:1–6.

[146] Drisdell, W. S.; Poloni, R.; McDonald, T. M.; Pascal, T. A.; Wan, L. F.; Pemmaraju, C. D.; Vlaisavljevich, B.; Odoh, S. O.; Neaton, J. B.; Long, J. R.; Prendergast, D.; Kortright, J. B. Probing the mechanism of CO_2 capture in diamine-appended metal–organic frameworks using measured and simulated X-ray spectroscopy. *Phys. Chem. Chem. Phys.* **2015,** *17,* 21448–21457.

[147] Bagge-Hansen, M. *et al.* Potential-induced electronic structure changes in supercapacitor electrodes observed by in operando soft x-ray spectroscopy. *Adv. Mater.* **2015,** *27,* 1512–1518.

[148] Schwartz, C.; Nordlund, D.; Weng, T.-C.; Sokaras, D.; Mansfield, L.; Krishnapriyan, A. S.; Ramanathan, K.; Hurst, K. E.; Prendergast, D.; Christensen, S. T. Electronic structure study of the CdS buffer layer in CIGS solar cells by X-ray absorption spectroscopy: Experiment and theory. *Sol. Energy Mater. Sol. Cells* **2016,** *149,* 275–283.

[149] Su, G. M.; Patel, S. N.; Pemmaraju, C. D.; Prendergast, D.; Chabinyc, M. L. First-principles predictions of near-edge x-ray absorption fine structure spectra of semiconducting polymers. *J. Phys. Chem. C* **2017,** *121,* 9142–9152.

[150] Altman, A. B.; Pemmaraju, C. D.; Alayoglu, S.; Arnold, J.; Booth, C. H.; Braun, A.; Bunker, C. E.; Herve, A.; Minasian, S. G.; Prendergast, D.; Shuh, D. K.; Tyliszczak, T. Chemical and morphological inhomogeneity of aluminum metal and oxides from soft x-ray spectromicroscopy. *Inorg. Chem.* **2017,** *56,* 5710–5719.

[151] Carravetta, V.; Plashkevych, O.; Ågren, H. A screened static-exchange potential for core electron excitations. *Chem. Phys.* **2001,** *263,* 231–242.

[152] Fransson, T.; Brumboiu, I. E.; Vidal, M. L.; Norman, P.; Coriani, S.; Dreuw, A. XABOOM: An x-ray absorption benchmark of organic molecules based on carbon, nitrogen, and oxygen 1s $\rightarrow \pi^*$ transitions. *J. Chem. Theory Comput.* **2021,** *17,* 1618–1637.

[153] Plekan, O.; Feyer, V.; Richter, R.; Coreno, M.; de Simone, M.; Prince, K. C.; Trofimov, A. B.; Gromov, E. V.; Zaytseva, I. L.; Schirmer, J. A theoretical and experimental study of the near edge X-ray absorption fine structure (NEXAFS) and X-ray photoelectron spectra (XPS) of nucleobases: Thymine and adenine. *Chem. Phys.* **2008,** *347,* 360–375.

[154] Hirao, K.; Nakajima, T.; Chan, B.; Song, J.-W.; Bae, H.-S. Core-level excitation energies of nucleic acid bases expressed as orbital energies of the Kohn–Sham density functional theory with long-range corrected functionals. *J. Phys. Chem. A* **2020,** *124,* 10482–10494.

[155] Schnack-Petersen, A. K.; Tenório, B. N. C.; Coriani, S.; Decleva, P.; Tross, J.; Ramasesha, K.; Coreno, M.; Totani, R.; Röder, A. Core spectroscopy of oxazole. *J. Chem. Phys.* **2023,** *157,* 214305:1–14.

[156] Sodhi, R. N. S.; Brion, C. E. High resolution carbon 1*s* and valence shell electronic excitation spectra of *trans*-1,3-butadiene and allene studied by electron energy loss spectroscopy. *J. Electron Spectrosc.* **1985,** *37,* 1–21.

[157] Turci, C. C.; Urquhart, S. G.; Hitchcock, A. P. Inner-shell excitation spectroscopy of aniline, nitrobenzene, and nitroanilines. *Can. J. Chem.* **1996,** *74,* 851–869.

[158] "Ohio Supercomputer Center", http://osc.edu/ark:/19495/f5s1ph73.

Table of Contents Graphic